Journal of Asian Earth Sciences 239 (2022) 105403

Contents lists available at ScienceDirect

Journal of Asian Earth Sciences

journal homepage: www.elsevier.com/locate/jseaes

The role of fluid mixing in the formation of vein-type Zn-Pb deposits in eastern Guizhou Province, SW China: Insights from elemental compositions and chlorine isotopes of fluid inclusions

Lin Xu [a], Chongguang Luo [b,*], Hanjie Wen [c,d,*], Zhengbin Zhou [a], Jeffrey de Fourestier [a]

[a] State Key Laboratory of Nuclear Resources and Environment, East China University of Technology, Nanchang 330013, Jiangxi, China
[b] State Key Laboratory of Ore Deposit Geochemistry, Institute of Geochemistry, Chinese Academy of Sciences, Guiyang 550081, China
[c] School of Earth Sciences and Resources, Chang'An University, Xi'an 710054, China
[d] College of Earth and Planetary Sciences, University of Chinese Academy of Sciences, Beijing 100049, China

ARTICLE INFO

Keywords:
Fluid mixing
Vein-type Zn–Pb deposits
Fluid inclusions
Ore deposition
Chlorine isotopes
Guizhou Province

ABSTRACT

Numerous hydrothermal vein-type Zn–Pb deposits worldwide are characterized by low-temperature metallogeny, no spatial relationship with plutons, and strong water-rock interaction, which result in the difficulty of constraining the fluid origin and the process of ore formation by traditional geochemistry. In this study, we employ chemical and chlorine isotopic composition of bulk fluid inclusions from ore-bearing and ore-barren quartz veins to constrain the possible sources of ore-forming fluids and the process of metal precipitation in the hydrothermal systems of the economic vein-type mineralization in eastern Guizhou Province, SW China. Our new geochemical data are indicative of two end-members in the systems, one identified in the ore-bearing veins with high K/Na, Li/Na, Cl/Br ratios, and δ^{37}Cl values representing magmatic hydrothermal fluids, another distinguished in the ore-barren veins with low Cl/Br ratios and δ^{37}Cl values representing evaporated seawater. We conclude there is a systematic variation of these geochemical data as the results of the mixing between the former and the latter end-member. In the meantime, the mixing is quantitively assessed to study the mixing volume ratios of both end-members. Based on our data and our own previous study, a genetic fluid mixing model involving the magmatic hydrothermal fluids related to deep magma activity and the evaporated seawater is established for the formation of the vein-type Zn–Pb deposits. This study provides a novel geochemical approach for recognizing hydrothermal mineralizing systems.

1. Introduction

Hydrothermal vein-type deposits have made an important contribution to the global supply of Au, Ag, Pb, Zn, Sb, and Cu metals (e.g., Bouabdellah et al., 2009; Ouyang et al., 2014). The ore-forming fluids of these deposits are commonly experienced a fluid migration from their metal sources, and finally upwelling along fractures into available locations for metal precipitation and accumulation (Large et al., 2016). It is well documented that numerous vein-type Zn–Pb deposits have a closely genetic relation to adjacent magmatic systems in many ore districts worldwide, such as the Main Stage veins at Butte, USA (Rusk et al., 2008), the base metal veins at Morococha, Peru (Catchpole et al., 2015), and the base metal veins in Inner Mongolia, SW China (Zhai et al., 2018). In contrast, some deposits do not appear to have a spatial and genetic association with granitic intrusions (de Sá et al., 2019), which would be hidden or corroded during the process of geologic evolution history. The fluid sources and metal deposition mechanism usually remain controversial, because their primary geochemical signatures may be changed by water-rock interaction during the fluid migration, or be diluted by extraneous fluids (meteoric water, metamorphic fluids) (Fusswinkel et al., 2013; Yang et al., 2015; Walter et al., 2019).

Cooling, boiling, mixing, and water-rock reaction are suggested to be the principal causes of the metal deposition in vein-type deposits (Yardley and Bodnar 2014, and references therein). The mixing of two fluids is an efficient mechanism for base metals deposition, this is in consideration of chemical-physical conditions of a macroshift of the hydrothermal mechanism (Palero et al., 2003). Generally, hydrothermal fluids originating from deep-seated magma are thought to be hotter and

* Corresponding authors at: State Key Laboratory of Ore Deposit Geochemistry, Institute of Geochemistry, Chinese Academy of Sciences, Guiyang 550081, China.
E-mail addresses: luochongguang@vip.gyig.ac.cn (C. Luo), wenhanjie@vip.gyig.ac.cn (H. Wen).

https://doi.org/10.1016/j.jseaes.2022.105403
Received 3 April 2022; Received in revised form 7 September 2022; Accepted 12 September 2022
Available online 17 September 2022

metal-rich in metallogenic systems, whereas other extraneous fluids are cooler and metal-poor (Zhai et al., 2018; Xiong et al., 2019). Traditional isotope geochemistry (δD, $\delta^{18}O$, $\delta^{34}S$), fluid inclusions microthermometry, and hydrogeological simulation are commonly employed to understand fluid mixing during the ore-forming processes (e.g., Fekete et al., 2016; Van Daele et al., 2018; Walter et al., 2019). However, many studies have shown that traditional isotopes seldom provide a robust constraint with the accumulation of the isotopes data (Gleeson et al., 2008; Yang et al., 2015). This is because that various isotopic exchanges and fractionation from water-rock interaction, mineral precipitation and phase separation would occur during fluid migration and evolution, which results in the dramatically change isotopic compositions of fluids. Also, the overlap of several potential isotopes budgets causes the complexity and uncertainty of fluid tracing. Currently, chemical and nontraditional isotopic signatures from fluid inclusions solutes have been increasingly recognized as a new and alternative tool.

As the most important metal complexing ligand in hydrothermal fluids, Cl concentrations in fluids affect the solubility and transport of a wide range of metals, such as Zn, Pb, and Cu (Yardley and Bodnar 2014; Hsu et al., 2019). Chlorine isotopes have been proved to be a powerful tracer for investigating the origin and evolution of ore-forming fluids (e.g., Banks et al., 2000 and 2002; Richard et al., 2011; Andersson et al., 2019), such as evaporated seawater, dissolution of halides, and magmatic fluids. The current analysis of $\delta^{37}Cl$ values mainly comes from fluid inclusions data obtained by bulk crush-leach ore-stage minerals, although this approach risks the interferences from secondary fluid inclusions. The discussion of chlorine isotopes is based on the published geological database, including modern seawater (0.0 ‰) (Eastoe et al., 2007), evaporated seawater (−1.0 ‰ to − 0.3 ‰) (Richard et al., 2011), granite-related hydrothermal fluids (~+1.0 ‰ to + 2.5 ‰) (Banks et al., 2000; Andersson et al., 2019), and mantle (<−1.4 ‰) (Bonifacie et al., 2008). Owing to the low Cl abundance in most minerals relative to crustal fluids, Cl removed or released by minerals could be negligible for the overall Cl supply present in a fluid-dominated system and does not

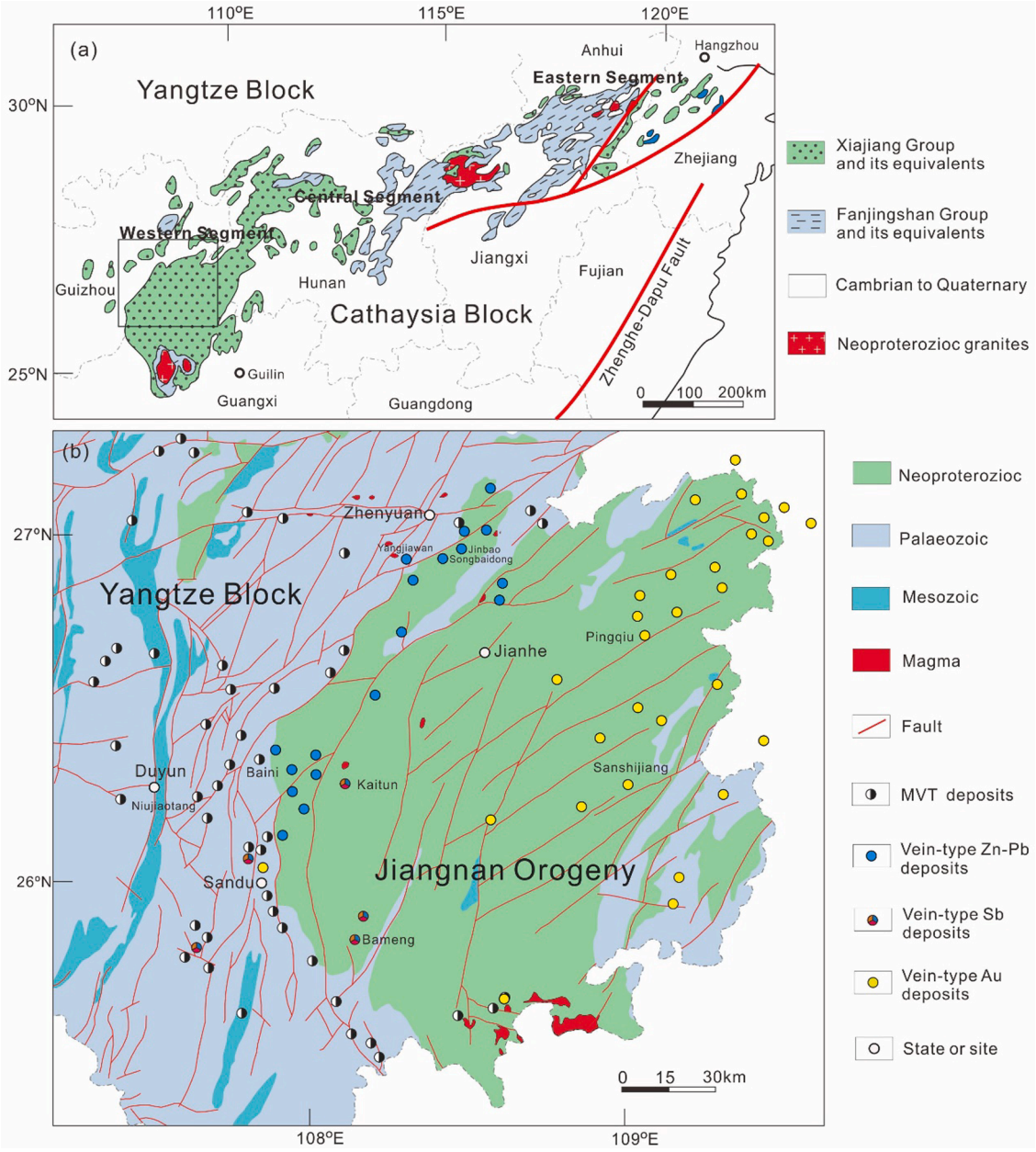

Fig. 1. (a) Simplified geological map of the Jiangnan orogenic belt and adjacent regions (modified from Wang et al., 2007); (b) Geological map showing the regional tectonic frame of eastern Guizhou province, the igneous units, and major vein-type and MVT deposits (modified from Chen et al., 2005).

affect chlorine isotopic compositions (Richard et al., 2011; Andersson et al., 2019; Xu et al., 2021). Therefore, chlorine isotopic signatures of ore-forming fluids should reflect the acquisition of salinity in the fluids or the fractionation mechanism.

Several vein-type Zn–Pb deposits have been identified in eastern Guizhou Province by drilling over the past two decades, and constitute of the important part of Xiangxi–Qiandong polymetallic metallogenic belt (e.g., Chen et al., 2005; Zhou et al., 2017 and 2021; Xu et al., 2018). These vein-type deposits share common geological characteristics: (1) The veins are composed of sphalerite, galena, chalcopyrite, and pyrite in a gangue of quartz with minor calcite; (2) The veins are hosted in the Neoproterozoic volcanic clastic rocks and sandstone–siltstone; (3) The mineralization is dominated by zinc and lead, accompanied by various concentration of copper, gallium, and indium; (4) Regional faults significantly control the distribution of this type deposits. No granitic intrusion outcrop have been documented around these deposits. Whether or not the Zn–Pb vein mineralization is related to deep magmatic activity and the ore deposition mechanism has been the source of some controversy (e.g., Zhou et al., 2017; Xu et al., 2018). Here, we present the results of elemental and Cl isotopic compositions of ore-stage fluids to constrain the sources of the hydrothermal fluids and the key controls on ore mineral precipitation. In turn, this information provides new constraints on genetic models for vein-type Zn–Pb mineralization, with concomitant implications for zinc-lead exploration.

2. Regional geology

Eastern areas of Guizhou Province are located in the western segment of the Jiangnan orogenic belt (Fig. 1a). The Jiangnan orogenic belt is 1500 km in length, 200 km in wide. It represents the suture zone between the Yangtze and Cathaysia blocks in South China, and can be divided into three tectonic domains, including the eastern, central and western segments (Li et al., 2009; Zhao et al., 2011). The belt was formed through complex orogenic processes including ocean-ocean subduction (ca. 970–880 Ma), arc-continent collision (880–860 Ma), ocean-continent subduction, and back-arc basin deposition (860–825 Ma) (e.g., Wang et al., 2007). The initial amalgamation of the Yangtze and Cathaysia blocks is considered to have occurred ca. 830 Ma along the Jiangnan orogenic belt (Li et al., 2009). Accompanying the breakup of the South China plate ca. 820 Ma, the tectonic setting transformed from the compression of these blocks to intracontinental extension (Yao et al., 2012).

Eastern areas of Guizhou Province are characterized by a series of NE-, NNE- and EW-trending folds and faults, which constrain the distribution of most of deposits (Fig. 1). Collision of the Yangtze and Cathaysia blocks at the Caledon event (ca. 415–512 Ma) resulted in deformation and metamorphism of the early strata in a NE direction, and molasse basin facies basal conglomerate sedimentation during the early Paleozoic (Wang et al., 2013). Next, Intracontinental orogeny of the South China Plate during the Yanshan event (ca. 180–160 Ma) laid out the structural architecture across the western segment of the Jiangnan orogenic belt at present (Mao et al., 2014), and was the cause of many uplifts and depressions that overprint earlier folds and faults.

The oldest strata exposed in the region studied are from the early Neoproterozoic Fanjingshan Group, which is equivalent to the Lengjiaxi Group in Hunan Province and to the Sibao Group in Guangxi Province. The Fanjingshan Group with a thickness of 7500–11600 m experienced greenschist-facies metamorphism and intensively deformation resulting in high-angle, tight, linear, and isoclinal overturned folds (Zhao et al., 2011). These strata are mainly composed of sandstone, siltstone, and argillaceous rocks intercalated with abundant volcanic rocks, and are unconformably overlain by rocks from the late Neoproterozoic Xiajiang Group in Guizhou Province, which is equivalent to the Banxi Group in Hunan Province and the Danzhou Group in Guangxi Province. The Xiajiang Group consists predominantly of a set of terrigenous clastic rocks interbedded with volcanic rocks. This Group has a maximum depositional age of ca. 815 Ma determined from tuff zircons (Gao et al., 2014). Numerous vein-type Au, Sb and Zn–Pb deposits in eastern Guizhou are hosted within the strata (e.g., Xu et al., 2017; Zhou et al., 2017; Xu et al., 2018). The Paleozoic strata are distributed along the southwestern margin of the Yangtze Block, and consist of the Cambrian, Ordovician, and Silurian neritic to littoral facies dominated by carbonates and siliciclastic rocks. The Mesozoic mud and sandstone overlie the Paleozoic sedimentary successions.

Three intermediate–acidic magmatic episodes have been recognized in the Jiangnan orogenic belt, including the Neoproterozoic, Paleozoic, and Mesozoic. The Neoproterozoic intrusion exposed in the western segments of the Jiangnan orogenic belt, known as the Motianling, was emplaced into the Neoproterozoic successions, and was believed to have been formed through the partial melting of the Neoproterozoic and/or older rocks. Zircon U–Pb dating of the Motianling intrusion yielded an age of ca. 830–795 Ma (Song et al., 2015). The Paleozoic (ca. 400–464 Ma) and Mesozoic (ca. 220–233 Ma) occurrences of S-type granite are mainly distributed in eastern and central segments of the Jiangnan orogenic belt (Chen et al., 2013; Wang et al., 2013). These bodies of granite are considered to have a genetic relationship with the W–Sn, Cu, Au, Sb, Pb–Zn mineralization in South China (Peng et al., 2003; Liu et al., 2017; Xu et al., 2017; Fu et al., 2020).

3. Ore deposit geology

The vein-type Zn–Pb deposits in eastern Guizhou include the Jinbao metallogenic district (Aihe, Bengchong, Laodu, and Pingmen deposits), the Nanshen metallogenic district (Nanshen and Paiwang deposits), and the Yangjiawan and Miaoniao deposits (Fig. 2). The identified Zn–Pb mineralization only occurs in two lithologically similar units of the Neoproterozoic Xiajiang Group. The lower Qingshuijiang Formation primarily consists of metamorphic tuff, siltstone, and tuff-sandstone with a thickness of approximately 2000 m. Zircon U–Pb dating of the formation yielded an age of 779.5 Ma (Qin et al., 2015). The upper Pinglue Formation is mainly composed of silt-bearing sericite slate, chloritic slate, and minor metamorphic siltstone interlayered with silt-bearing tuff. The thickness of the Pinglue Formation is approximately 1800 m. Zircon U–Pb dating of the formation yielded an age of 764.0 ± 6.3 Ma (Qin et al., 2015).

Igneous rocks exposed in the Jinbao ore district are lamproites, with emplaced within the Neoproterozoic slate and the Cambrian carbonates. Texturally, the lamproites can be subdivided into massive, star shaped point, and lamprophyric structure. These rocks consist of pyrope, olivine, and Cr-rich diopside with approximately 416 Ma of age constrained by bulk rock K–Ar dating (Fang et al., 2002). No exposed granite is found around the ore district. However, geophysical data suggested that many felsic intrusions lie beneath these deposits (Wang et al., 2009). In addition, according to the geological survey, Zn, Pb, and Cu concentrations within the strata overlying the intrusions are three to six times higher than the mean values of the upper crust (Yang and Liu 2014).

Dominant faults within the ore district include NE-trending normal faults and their secondary locally NS- and EW-trending faults (Fig. 2). The main Zn–Pb–(Cu) veins are located parallel to the NE-trending fault zone. Minor sulphide veins are emplaced into NS-trending fault zone. Specifically, the junction between anticlines and NS-trending faults are the most favourable structures for veins to occur. F1, F4, F5, F6, F7, F8, and F9 are characterized by extensional features, while F2 and F3 are characterized by compress-torsional features (Fig. 2). The F1 and F7 dip NW at 55° to 75° and 56° to 68°, and have been traced along the strike for distances of 2.2 km and 6.5 km, respectively. The most important sulphide mineralization in this district is dominantly structurally controlled by the F1 and F7 faults.

These deposits have an average grade of 5.60 % Pb, 3.80 % Zn, and 0.09 % Cu (Zhou et al., 2017; Xu et al., 2018). Ore mainly occurs as quartz veins, sulphide breccias, and stock works along fractures.

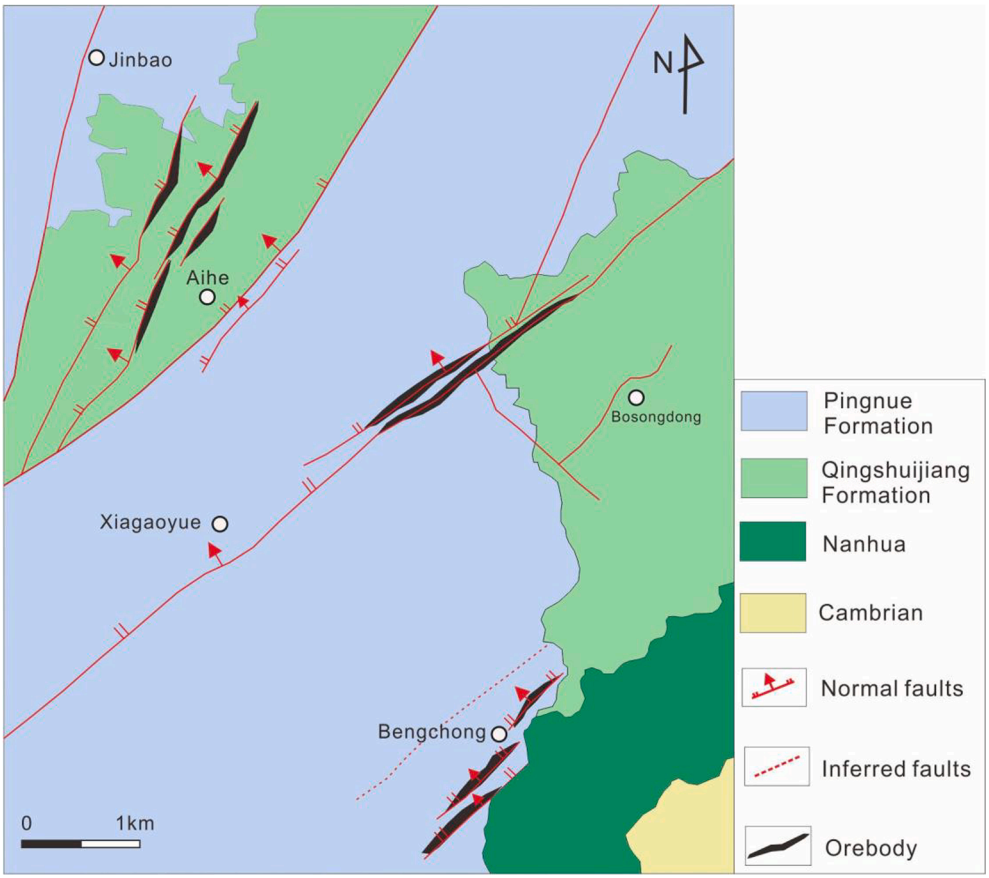

Fig. 2. (a) Geological map of the central Jinbao metallogenic district (Modified from Zhou et al., 2017).

Economic ore veins are 0.42–2.10 m in wide, and extend 0.4–120.0 m along the strike. Mineral assemblage is relatively simple, and contains sphalerite, galena, chalcopyrite, pyrite, quartz, calcite, a member of the chlorite group, and muscovite (sericite). Hydrothermal alteration occurs mainly on both sides of the major Pb–Zn mineralized veins, characterized by an assemblage of quartz, calcite, a member of the chlorite group, muscovite (sericite), and baryte. The Neoproterozoic host rocks have undergone intense silicification, which is closely associated with sulphide mineralization.

4. Sampling and methodology

4.1. Sample and pretreatment

Selecting representative samples is critical to ensure the data quality. In order to investigate the sources and evolution of the ore-forming fluids, we sampled quartz crystals associated with ore minerals using the crush-leach method to extract fluid inclusions leachates. >20 samples come from four deposits, including the Jinbao metallogenic district (the Bengchong and Pingmen deposits), the Nanshen metallogenic district (the Paiwang deposit), and the Yangjiawan deposit. Description of samples for extraction of fluid inclusions are showed in Table 1 and Fig. 3a-i. Many barren quartz veins contain spot, disseminated, and veinlet-like sphalerite. In contrast, quartz from ore-bearing hydrothermal veins is typically cemented by sphalerite, or crystallized around breccias/fragments of host rocks with sulphides filling in the vug and interstitial of quartz. Some sulphides are precipitated on the both sides along quartz vein. The paragenetic sequence of ore and gangue minerals has been studied through field observation as well as the investigation of hand specimens or under microscope in Zhou et al., 2017. So, these samples are likely to host fluid inclusions that are relicts of fluids responsible for the mineralization.

Fluid inclusions have been analysed microthermometrically in quartz from the main mineralization (Zhou et al., 2017). Petrographic studies show that many primary fluid inclusions occur randomly or regularly along growth bands or healed fissures in quartz crystals and they occasionally exist in isolation. They are rod-shaped, oval, irregular or display negative crystal shapes, and mostly range in length from 3 to 10 μm with minor amounts exceeding 10 μm (Fig. 4a-f). Secondary fluid inclusions occasionally occurs in microfissures cutting through the hosted quartz crystals (Fig. 4d). Fluid inclusions have two phases (liquid + vapor) with the vapor phase ranging from 5 to 10 vol% of the whole inclusion. Most inclusions are too small to measure microthermometry. Microthermometric analyses reveal that homogenization temperatures vary from 102 to 198 °C (average in 133 °C) in the Bengchong deposit, 105 to 238 °C (average in 164 °C) in the Pingmen deposit, 132 to 183 °C (average in 150 °C) in the Paiwang deposit, and 119 to 132 °C (average in 126 °C) in the Yangjiawan deposit, respectively. From the Bengchong to the Yangjiawan deposit, fluid salinities vary from 10.74 to 26.64 wt% (average in 15.80 wt%), 2.90 to 26.30 wt% (average in 17.60 wt%), 2.73 to 12.88 wt% (average in 7.66 wt%), and 13.55 to 21.95 wt% (average in 20.36 wt%) NaCl equiv, respectively. Fluid inclusions trapped in quartz from the four vein-type Zn–Pb deposits have similar homogenization temperature, but variable salinity which could be classified as two intervals: 2.0 to 6.0 wt% NaCl equiv and 14.0 to 27.0 wt% NaCl equiv.

All samples were crushed and sieved to a grain-size of 20–40 mesh. They were handpicked under a binocular microscope. Selected quartz grains were washed using 2 wt% HNO_3 in a ultrasonic bath for 1 h. After being dried in an oven, cleaned samples were weighed and transferred into a corundum mortar to which was added 35 mL ultrapure water (>18.2 MΩ). The planetary ball mill equipped with four corundum

Table 1
Basic information of the collected samples.

Deposits	Salinity and homogenization temperature		Description	Samples
Bengchong	102 to 198 °C 10.74 to 26.64 wt % NaCl equiv	Ore-barren vein	Quartz veins contain spot, disseminated and veinlet-like sphalerite	BC-2-3, BC-3-1, BC-3-2, BC-3-3, BC-3-Kd-2
		Ore-bearing vein	Sulphides (sphalerite, galena and pyrite) are filled into the vug and interstitial of quartz vein	BC-3-4, BC-3-Kd-7, BC-5-2, BC-5-4, BC-5-Pd-1, BC-5-Pd-4
			Quartz crystals are cemented by sphalerite	BC-3-5, BC-5-1
			Minor chalcopyrite occurs in sulphide-dominated quartz vein	BC-5-5, BC-5-6, BC-5-11
Pingmen	105 to 238 °C 2.90 to 26.30 wt% NaCl equiv	Ore-bearing vein	Sulphides grow the both sides along quartz vein	PM, PM-1-15-1, PM-1-13, PM-1-10
Paiwang		Ore-barren vein	Quartz-calcite veins contain spot, disseminated and veinlet-like sphalerite	PW-4, PW-6-3
	132 to 183 °C 2.73 to 12.88 wt% NaCl equiv	Ore-bearing vein	Sulphides (sphalerite, galena and pyrite) are filled into the vug and interstitial of quartz vein	PW-12
Yangjiawan	119 to 132 °C 13.55 to 21.95 wt % NaCl equiv	Ore-barren vein	Quartz-calcite veins contain spot, disseminated and veinlet-like sphalerite	YJW-2

mortars was used to crush the quartz grains into fine powder to release fluid inclusions into the water. The crush-leach process takes about 40 min to satisfy the all extraction of fluid inclusions preserved within the quartz crystals. The collected solutions were then filtered using 0.2 μm nylon filters for removal of any particulates before analysis. Notably, the interpretation of the data in terms of fluid mixing is based on the implicit assumption that the chemical and isotopic signatures are not the result of mixing of distinct fluid inclusion populations during the extraction of fluid inclusion leachates.

4.2. Concentration analysis

Analysis of the sample solutions was carried out at the State Key Laboratory of Environment Geochemistry, Institute of Geochemistry, Chinese Academy of Sciences. Halogens (Cl and Br) were determined using a Dionex ICS–90 ion chromatograph. Na, K, Mg, and Ca were measured by inductively coupled plasma optical emission spectrometry (ICP–OES, Varian Vista MPX). Li was determined via NexION 300X ICP–MS. Uncertainty in all element concentrations is better than 10 %.

4.3. Cl isotopes

Before Cl isotopes could be determination, Cl in sample solutions were required to undergo chemical preparation. Owing to negligible NO_3^- and SO_4^{2-} in the solutions, the purification described in Xiao and Zhang (1992) is not necessary. The conversion of NaCl or XCl_2 (X = e.g., Mg and Ca) into CsCl was carried out using H- and Cs-form resin. The samples were first concentrated in 50–100 μL to 7 mL Teflon breakers. Then, a connection in series between a prepared 0.2 mL column of H-form resin and a 0.2 mL column of Cs-form resin was employed to obtain the CsCl solutions. The conversion processes take place in the two form resin columns-$H^+ + Cl^- \rightarrow HCl$ for the former and $Cs^+ + HCl \rightarrow CsCl + H^+$ for the latter. A pH test strip was used to monitor whether the conversion has succeeded. If the colour of the strip changed into red, the sample was unsuccessful, and needed for re-preparation follow the steps above. To satisfy the determination requirement, a minimum of 50 μg of Cl in the obtained solutions were concentrated into 20–30 μL at a temperature range of 40–60 °C for subsequent isotope ratio measurement.

Chlorine isotopic measurement was performed at the Qinghai Institute of Salt Lakes, Chinese Academy of Sciences. The positive thermal ionization mass spectrometry (P–TIMS) based on the Cs_2Cl^+ with a graphite load was used to measure the $^{37}Cl/^{35}Cl$ ratios in all samples. This method was described in detail in Xiao and Zhang (1992) and Luo et al., (2012). Firstly, a 2.5 μL graphite slurry in 80 % ethanol and 3 μL concentrated sample solutions containing ~ 10 μg Cl were successively introduced into the centre of an outgassed Ta filament. The solution was then dried using a current of 1 amp for 1.5 min in a clean air flow unit. Next, the prepared samples were placed in the ion source of the mass spectrometer. Isotopic ratio was analysed when the ion source placed in a vacuum of$<2.5 \times 10^{-7}$ mbar. Intensity of the Cs_2Cl^+ ion was adjusted to 4×10^{-12} A by controlling the filament current. The data were simultaneously obtained on Faraday cup C and H1 by collecting the ion flow with mass numbers of 301 ($^{133}Cs^{235}Cl^+$) and 303 ($^{133}Cs^{237}Cl^+$). All data were reported in per mil delta notation relative to ISL 354. Repeated analysis of Cl isotopes standard (ISL 354 NaCl) yielded an average $^{37}Cl/^{35}Cl$ ratio of 0.319030 ± 0.000071 (2σ). Chlorine isotopic compositions of fluid inclusions leachates in this study were finally expressed as follows.

$$\delta^{37}Cl(‰)=\{[(^{37}Cl/^{35}Cl)_{Sample}/(^{37}Cl/^{35}Cl)_{Standard}]-1\} \times 1000.$$

5. Results

All ion concentrations in the fluid leachates are reported in Table S1. Cation/anion molar ratios ($^+\Sigma/^-\Sigma$) of most of the samples analysed from the four deposits studied are close to 1, indicating that sufficient ions were present to achieve charge balance. However, a few samples, such as BC-3-3, PW-4, PW-12, PM-1-13, PM-1-10, and YJW-2, clearly display an excess of cations. As well, these samples have an extremely high Ca concentration. Considering that calcite is a main gangue mineral at the four deposits, it is reasonable to conclude that calcite inclusions within quartz grains provided the extra Ca in the leachates during crush-leach process. This aspect is similar to Banks et al. (2002). They analysis excluded Ca to avoid interference from calcite inclusions, and demonstrated a deficiency of cations needed to achieve the charge balance. Therefore, Ca concentrations in such samples are excluded from the discussion below.

Ore-forming fluids are represented by fluid inclusions leachates extracted from the quartz grains. Chemistry of these fluid inclusions from the four deposits is dominated by Na–Ca–K–Mg and Cl ions. These ion concentrations constitute > 80 % of the major cations and anions. Absolute concentrations in the leachates are associated with sample weight, leachate volume, and the number of primary fluid inclusions, which led to ion concentrations in the leachates, are apart from those in fluid inclusions. However, elemental ratios (e.g., Cl/Br, Li/Na, Ca/K) in the leachates are comparable to fluid inclusions (Banks et al., 2002; Heijlen et al., 2008; De Graaf et al., 2020). All elemental ratios (molar) in this study are shown in Table 2. Samples exhibit a relative narrow range of K/Na ratios, from 0.01 to 0.14 in the Bengchong deposit, from 0.02 to 0.07 in the Pingmen deposit, from 0.08 to 0.47 in the Paiwang

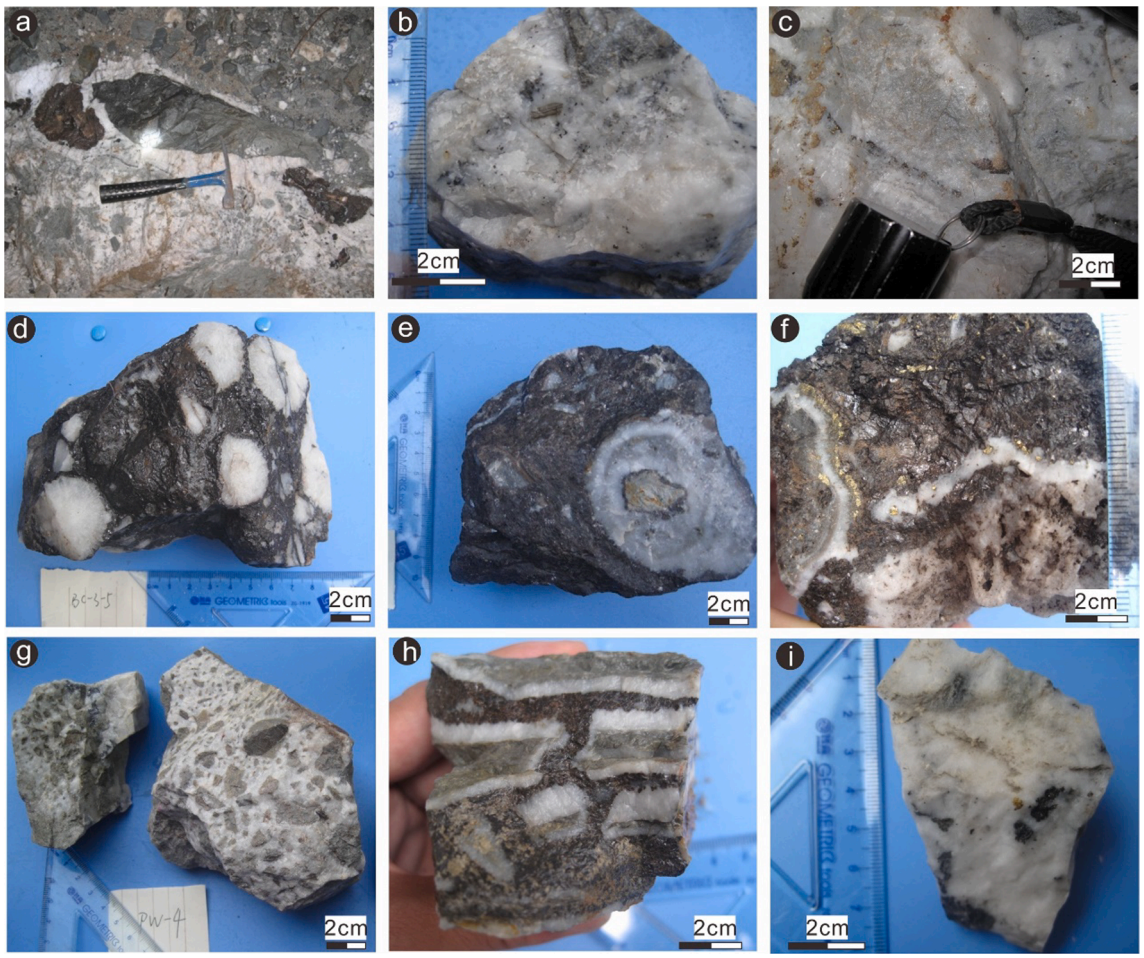

Fig. 3. (a) Massive Zn-Pb ore and host rock breccias in a NE-trending mineralized vein; (b) Spot and disseminated sphalerites in a barren vein; (c) Comb-textured quartz with sulphides veinlet filling in; (d) Quartz nodules in sphalerite vein; (e) Quartz is crystalized around host rock breccia, and overgrown by sphalerite; (f) Quartz veins in sulphide vein; (g) Host rock breccias in a barren vein; (h) Sphalerite infills in the interspace of quartz; (i) Minor sulphide grains in a barren quartz-calcite vein.

deposit, and 0.08 in the Yangjiawan deposit. By contrast, most samples show a large variation of Ca/K ratios, from 1.57 to 32.92 in the Bengchong deposit, 0.78 to 20.47 in the Pingmen deposit, and 23.43 in the Paiwang deposit. Only one sample (BC-5-Pd-1) possesses a ratio > 621.00. In addition, a large variation of Li/Na ratios ($\times 10^{-3}$) is present, from 17.13 to 155.29 in the Bengchong deposit, 126.47 to 176.37 in the Paiwang deposit, 40.00 to 1329.00 in the Pingmen deposit, and 6.35 in the Yangjiawan deposit. These ratios will be compared to those from published natural fluid ratios in the following discussion.

Cl/Br ratios of the fluid inclusions leachates range from 266.54 to 1566.94 in the Bengchong deposit, from 161.83 to 638.64 in the Pingmen deposit, from 328.64 to 1244.64 in the Paiwang deposit, and 467.65 in the Yangjiawan deposit. δ^{37}Cl values display a significant variation, from −0.79 ‰ to +2.50 ‰ in the Bengchong deposit, from +0.25 ‰ to +0.82 ‰ in the Pingmen deposit, from +0.18 ‰ to +1.10 ‰ in the Paiwang deposit, and +0.94 ‰ in the Yangjiawan deposit. Most samples possess predominantly positive δ^{37}Cl values. Some values from the Bengchong deposit are slightly lower than that of modern seawater (0.0 ‰).

6. Discussion

Mixing of two-component or multicomponent fluids is usually cited as a critical process for ore metal deposition mechanism in the hydrothermal vein-type deposits (e.g., Bons et al., 2014; Beaudoin and Chiaradia, 2016; De Graaf et al., 2020). This process is supported by numerous geochemical and geological evidences. The mixing is comparable to the model of this study. Fluids from different reservoirs often display distinct differences in temperature, salinity, chemical composition, and oxygen fugacity (e.g., Wilkinson, 2001; Williams-Jones et al., 2010; Bons et al., 2014). In numerous studies, evidence is presented that mixing metal-rich fluids and metal-poor fluids forms these base metals ore deposits (Bons et al., 2014; Zhai et al., 2018; Walter et al., 2019, and references therein). Inasmuch as the hydrothermal vein-type Zn–Pb deposits in eastern Guizhou have no direct spatial relationship with intermediate–acidic rock, the ore-forming fluids would be magmatic, meteoric, or other crustal water. Based on oxygen and carbon isotope data, Yang and Liu (2014) proposed that the ore-forming fluids have a predominately magmatic origin. Recently, it has been demonstrated that two fluids are readily distinguished by hydrogen, oxygen, lithium isotopic composition of fluid inclusions in quartz (−126 ‰ to −80 ‰, +0.2 ‰ to +4.2 ‰, +8.2 ‰ to +16.3 ‰, respectively), and fluid inclusions microthermometry (Zhou et al., 2017; Xu et al., 2018). These studies suggested that deep − seated magmatic hydrothermal fluids may be responsible for the mineralization, while other crustal fluids (e.g., meteoric water) derived from the surface make a significant contribution to the hydrothermal system during the late ore-forming process.

Differences in elemental ratios (K/Na, Ca/K, Li/Na, and Cl/Br ratios) and chlorine isotope data distinctly indicate the presence of at least two fluids for the fluid system in the vein-type Zn–Pb deposits. Fig. 5a demonstrates a logarithm negative relationship between K/Na ratios and Ca/K ratios. High K/Na, low Ca/K ratios are typical of magmatic

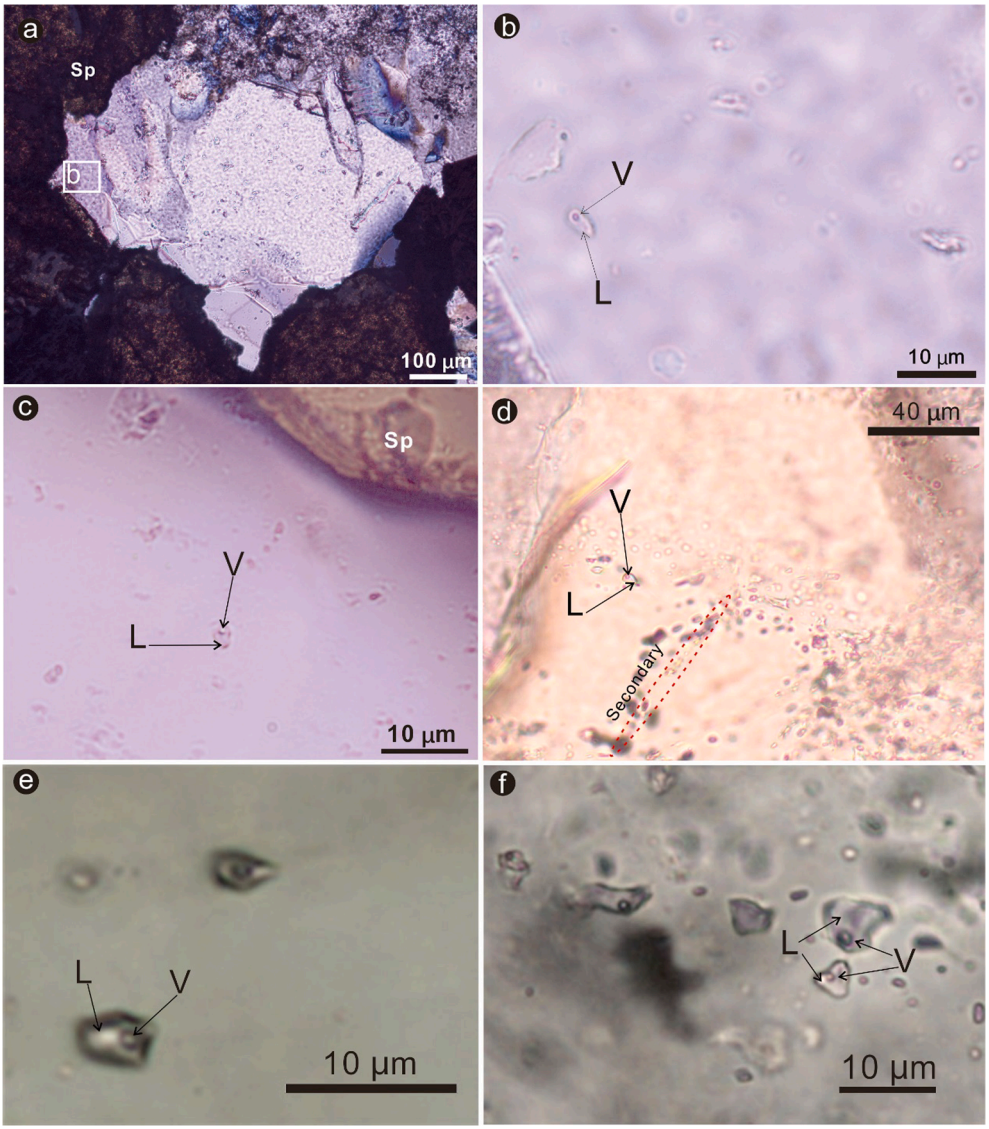

Fig. 4. Photomicrographs of representative fluid inclusions in quartz. (a, b, c) Primary irregular L + V fluid inclusions randomly distributed in quartz crystals associated with sphalerite. (d) A group of fluid inclusions in quartz crystals with minor secondary fluid inclusions filling in microfissures. (e, f) Primary irregular rod-shaped and oval L + V fluid inclusions. L = liquid, V = vapor.

hydrothermal fluids (Wilkinson 2001), whereas low K/Na, high Ca/K ratios probably delimit compositions of fluids in sedimentary environment, such as basinal brines derived from evaporated seawater (Heijlen et al., 2008; Yardley and Bodnar, 2014; Shu et al., 2017). These crustal fluids without relationship to magmatic activity are expected to have an increased Ca concentration through Na–Ca exchange reactions during the fluid migration, which is readily available in the western segment of Jiangnan orogenic belt where carbonate formations occur widely (Fig. 1). The above data are best interpreted by the fluid mixing between magmatic hydrothermal fluids and evaporated seawater. As shown in Fig. 5b, some samples are plotted into or near to the field of magmatic hydrothermal fluids, and the majority of samples has Li/Na ratios higher than typical basinal fluids. It implies high Li/Na ratios in primary ore fluids, which is also supported by strong enrichment of Li in sphalerite (22.6–160.0 μg/g, mostly 80–160.0 μg/g) (Zhou and Wen 2021). We conclude that the primary ore fluids are diluted by basinal fluids with low Li/Na ratios and Li contents through the mixing, which results in the shift of Li/Na ratios from magmatic hydrothermal fluids to basinal fluids (Fig. 5b). The samples with the high Li/Na, K/Na ratios, and low Ca/K ratios are comparable to the deposits related to granitic magma, such as El Mochito, Honduras (Williams-Jones et al., 2010; Samson et al., 2008), and Baiyinnuo'er, China (Shu et al., 2017). The samples with the low Li/Na, K/Na ratios, and high Ca/K ratios are comparable to the deposits that have the fluids sources related to the evaporated seawater, such as the Irish midlands (Banks et al., 2002), Niujiaotang, China (Ye et al., 2012), the Schwarzwald, Germany (Fusswinkel et al., 2013), and the Harz mountains (De Graaf et al., 2020).

Distribution of Cl/Br ratios and δ^{37}Cl values (Fig. 6) is also suggestive of the mixing of two fluids from different reservoirs in this hydrothermal system. It has been previously shown that fluid inclusions are characterized by a large variation of salinity (Zhou et al., 2017), hinting that the two fluids have greatly contrasting properties based on salt sources. Halite dissolution can be ruled out as the main method for obtaining the observed fluid salinity. When ore fluids pass through evaporites to attain their salinity, it is suggested to produce fluids with Cl/Br molar ratios higher than 4000 and δ^{37}Cl values about 0.0 ‰ (Fontes and Matray, 1993; Eastoe et al., 2007; Eggenkamp et al., 2019). This a marked difference from the vast majority of results for the system observed in this study. Moreover, it is also supported from field investigation by the absence of evaporites in the sedimentary sequences. However, there is

Table 2
Results of chemical and chlorine isotopic compositions for leachates.

Sample		δ^{37}Cl(‰)	2SD	Cl/Br(M)	K/Na(M)	Ca/K(M)	Li/Na ($\times10^{-3}$, M)
BC-2-3	Ore-barren vein	0.31	0.21	441.75	0.09	2.45	27
BC-3-1	Ore-barren vein	−0.23	0.33	332.47	0.03	20.20	86
BC-3-2	Ore-barren vein	0.86	0.30	266.54	0.05	4.74	66
BC-3-3	Ore-barren vein	−0.79	0.23	434.50	<0.01	–	17
BC-3-4	Ore-bearing vein	0.70	0.32	267.64	0.14	1.57	56
BC-3-5	Ore-bearing vein	1.54	0.22	436.31	0.05	6.82	70
BC-3-Kd-2	Ore-barren vein	−0.30	0.29	332.07	0.06	5.83	27
BC-3-Kd-7	Ore-bearing vein	1.38	0.28	326.65	0.06	5.20	104
BC-5-1	Ore-bearing vein	–	–	>525.76	0.01	32.92	95
BC-5-2	Ore-bearing vein	1.30	0.26	387.28	0.11	2.01	44
BC-5-4	Ore-bearing vein	0.63	0.32	301.03	0.04	8.40	147
BC-5-5	Ore-bearing vein	0.63	0.33	270.38	0.04	8.86	82
BC-5-6	Ore-bearing vein	0.79	0.47	320.39	0.03	11.37	155
BC-5-11	Ore-bearing vein	2.05	0.13	330.18	0.04	8.64	77
BC-5-Pd-1	Ore-bearing vein	0.96	0.22	355.69	<0.01	>621.00	91
BC-5-Pd-4	Ore-bearing vein	2.50	0.23	>1566.94	0.07	4.02	97
PW-4	Ore-barren vein	0.18	0.10	>1244.64	0.07	–	126
PW-6-3	Ore-barren vein	0.57	0.13	328.60	0.02	23.43	176
PW-12	Ore-bearing vein	1.10	0.37	831.64	0.05	–	158
PM	Ore-bearing vein	-	–	161.83	0.19	20.74	991
PM-1-15-1	Ore-bearing vein	–	–	>226.87	0.29	0.78	1329
PM-1-13	Ore-bearing vein	0.25	0.27	>528.92	0.47	–	178
Continue							
Sample		**δ^{37}Cl(‰)**	**2SD**	**Cl/Br(M)**	**K/Na(M)**	**Ca/K(M)**	**Li/Na ($\times10^{-3}$, M)**
PM-1-10	Ore-bearing vein	0.82	0.14	638.64	0.08	–	40
YJW-2	Ore-barren vein	0.94	0.31	467.65	0.08	–	6

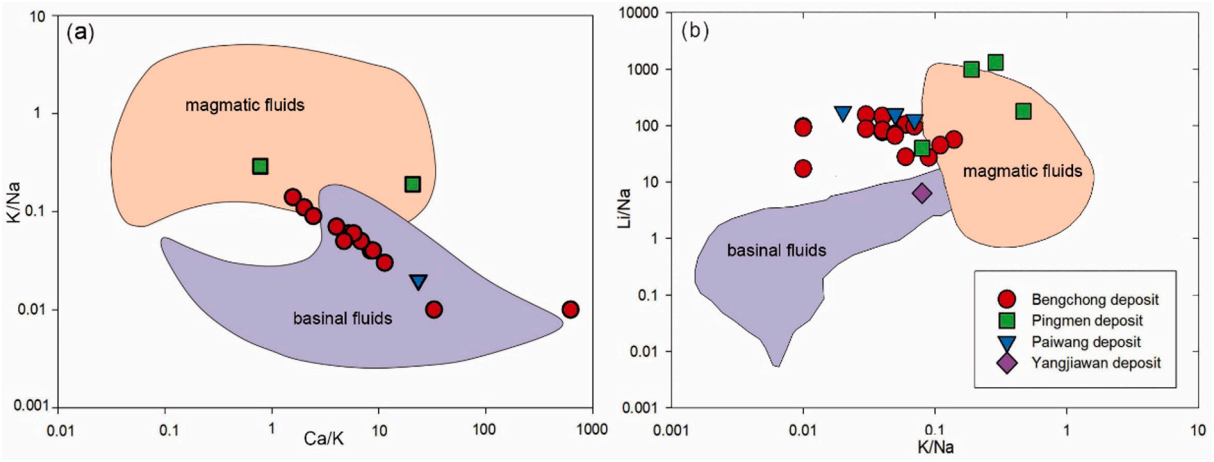

Fig. 5. (a) K/Na ratios plotted as a function of Ca/K ratios (Modified after Shu et al., 2017); (b) Li/Na ratios plotted as a function of K/Na ratios (Modified after Heijlen et al., 2008).

still one sample from ore-barren vein with Cl/Br molar ratios higher than 1244.64 and δ^{37}Cl values about 0.0 ‰. It could be interpreted to the assimilation of halite microcrystalline by the fluids during the late stage of ore-forming process. Based on a compilation of Cl/Br ratios (600 to 2000) and δ^{37}Cl values (+1.0 ‰ to + 2.5 ‰) from magmatic sources associated with granitic magmatism (Banks et al., 2000; Andersson et al., 2019), an important magmatic end-member is identified from the values from the ore-bearing vein. In contrast, some values of the ore-barren vein is similar to that of the evaporated seawater (50 to 300, −1.0 ‰ to − 0.3 ‰) with the evaporation progress reaching the end of precipitation of halite. This end-member is suggested to have values significantly lower than original seawater (649, 0 ‰) (Richard et al., 2011), which is the results of preferentially partition of Br and ^{35}Cl into the residual phase during the evaporation (Fontes and Matray, 1993; Eggenkamp et al., 1995; Luo et al., 2012). In addition, the variation tendency between δ^{37}Cl values and Cl/Br ratios in Fig. 6 cannot be attributed to fluid phase separation during the fluid evolution. Currently, there are two opposite views for the fractionation of Cl/Br ratios and Cl isotopes during the phase separation. One view suggested absence of Cl isotope fractionation and minor fractionation of Cl/Br ratios with slightly vapour partitioning of Br through experimental studies (e.g., Liebscher et al., 2006; Seo and Zajacz, 2016). Another view proposed occurrence of large fractionation of Cl isotopes (several per mil) and Cl/Br ratios due in the separation determined in fluid inclusions trapped in sphalerite, and ^{37}Cl and Br are intensively partitioned into the brine phase (Lüders et al., 2002). According to the former view, homogeneous fluid signatures should be well preserved during the phase separation. That is inconsistent with the results. If it is the latter case, a negative correlation between Cl/Br ratio and δ^{37}Cl values should be observed in our results, like Lüders et al., (2002). Both views do not account for the variation tendency. Thus, the fluid mixing between magmatic hydrothermal fluids and evaporated seawater is proposed to the critical mechanism for the precipitation of sulphides in the hydrothermal system.

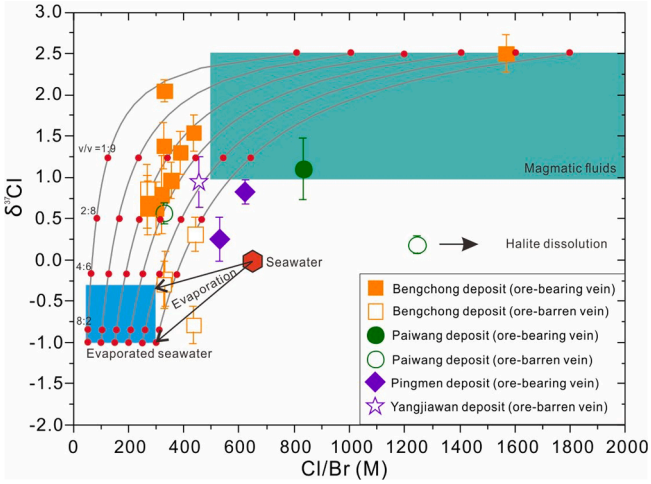

Fig. 6. $\delta^{37}Cl$ values plotted as a function of Cl/Br ratios (Evaporated seawater is sourced from Richard et al., 2011; Seawater is sourced from Eastoe et al., 2007; Magmatic fluids are sourced from Banks et al., 2000; Andersson et al., 2019). Grey lines are calculated, based on the mixing between evaporated seawater end-member and magmatic fluids end-member.

In the model, we calculate 6 mixing lines to fit the variation tendency between Cl/Br ratio and $\delta^{37}Cl$ values in Fig. 6. The selected endpoints of calculated curves are (300, −0.1; 1800, −2.5), (250, −0.1; 1600, −2.5), (200, −0.1; 1400, −2.5), (150, −0.1; 1200, −2.5), (100, −0.1; 1000, −2.5), and (50, −0.1; 800, −2.5), respectively. All of these endpoints are consistent with the published geological reservoirs. Furthermore, salinity ratio between evaporated seawater and magmatic fluids in studied hydrothermal system is fixed to 5 [$NaCl_{(evaporated\ seawate;\ es)}$/ $NaCl_{(magmatic\ fluid;mf)}$], based on the salinity range from previous microthermometric analyses (Zhou et al., 2017).

The concentration of Cl and Br of ore-forming fluids through the fluid mixing is then:

$$C(Cl) = \frac{C_{es,Cl} \times V_{es} + C_{mf,Cl} \times V_{mf}}{V_{es} + V_{mf}} \quad (1)$$

$$C(Br) = \frac{C_{es,Br} \times V_{es} + C_{mf,Br} \times V_{mf}}{V_{es} + V_{mf}} \quad (2)$$

$C_{es,Cl}$ = initial content of Cl in evaporated seawater;
$C_{es,Br}$ = initial content of Br in evaporated seawater;
V_{es} = volume of evaporated seawater;
$C_{mf,Cl}$ = initial content of Cl in magmatic fluids;
$C_{mf,Br}$ = initial content of Cl in magmatic fluids;
V_{mf} = volume of magmatic fluids;
$C_{es,Cl}/C_{mf,Cl} = 5$;
We set 't' as volume ratios between evaporated seawater and magmatic fluids ($t = V_{es}: V_{mf}$), $0 \le t \le 10$;
So, the Cl/Br ratios as a function of t is then:

$$Cl/Br = \frac{10 \times \omega \times \varphi \times (5 + 2 \times t)}{5 \times \varphi \times t + (10 - t) \times \omega} \quad (3)$$

(ω, φ) are the six Cl/Br ratios endpoints from the fields of magmatic hydrothermal fluids and evaporated seawater-(300, 1800), (250, 1600), (200, 1400), (150, 1200), (100, 1000), and (50, 1800), respectively.

Additionally, the $\delta^{37}Cl$ values of ore-forming fluids through the fluid mixing is then:

$$\delta^{37}Cl(‰) = \delta^{37}Cl(‰)_{es} \times \frac{C_{es,Cl} \times V_{es,Cl}}{(C_{es,Cl} \times V_{es,Cl}) + (C_{mf,Cl} \times V_{mf,Cl})} + \delta^{37}Cl(‰)_{mf} \times \frac{C_{mf,Cl} \times V_{mf,Cl}}{(C_{es,Cl} \times V_{es,Cl}) + (C_{mf,Cl} \times V_{mf,Cl})} \quad (4)$$

So, the $\delta^{37}Cl$ values as a function of t is then:

$$\delta^{37}Cl(‰) = \frac{50 - 15 \times t}{20 + 8 \times t} \quad (5)$$

The calculated curves in the binary diagram (Eq (3) versus. Eq5) provide a quantificational assessment for the fluid mixing. If the mixing occurs, data plotted in Eq (3) versus. Eq5 would tend to be distributed along these curves. The coupled variation of Cl/Br ratios versus $\delta^{37}Cl$ values from the hydrothermal vein-type Zn–Pb deposits in eastern Guizhou Province is reasonable consistent with these curves, which is evidence in favour of a fluid mixing process. Most of data fall in the field between v/v = 1:9 and 4:6. Thus, it is concluded that coefficient between evaporated seawater and magmatic fluids plays a considerable role to trigger the Zn–Pb mineralization. From another perspective, the results showed that fluid mixing between different end-members could be an important factor for generating variational $\delta^{37}Cl$ values from hydrothermal deposits, besides heterogeneity of crust, phase separation, and Cl losses through the precipitation of hydrous silicate minerals (e.g., biotite, scapolite, amphibole) in the previous researches (e.g., Gleeson et al., 2008; Nahnybida et al., 2009; Kusebauch et al., 2015; Andersson et al., 2019; Xu et al., 2021).

The isotopic and compositional variability from the fluid inclusions leachates provides a proxy for inhomogeneity of fluids trapped in quartz veins and fluid-mixing process at deposit scale. On the evidence available, a genetic model involving mixing of two fluids is established for the formation of the vein-type Zn–Pb deposits. In this model, ore-bearing, deep-seated magmatic hydrothermal fluids arose along reginal faults to shallower crustal levels, and mixed with ore-poor, surface-evaporated seawater in favourable positions (e.g., fractures, breccia zones of surrounding country rocks) for the precipitation of sulphides. In western segment of the Jiangnan orogenic belt, magmatic hydrothermal fluids were most likely released from magmatic activity at depth during the Caledonian tectono-thermal event (Zhou et al., 2017). These fluids were driven by tectonic forces transporting metals away from their sourced plutons, and passed through the huge thick sedimentary rocks in the region, such as the higher 7 km thick Xiajiang Group. We emphasize that the vein-type Zn–Pb deposits formed along faults and adjacent open space where both fluids gathered flowing in a local geologic environment. Combination of magmatic hydrothermal fluids and evaporated seawater resulted in the economic mineralization. We hold the promise for that the model provides significant implications for regional vein-type Zn–Pb exploration.

7. Conclusion

Elemental compositional and chlorine isotopic analyses of bulk fluid inclusions from quartz veins have been measured to elucidate the ore-forming fluid sources and metal deposition mechanism in eastern Guizhou Province. Significant variations in element and chlorine isotopes ratios suggest that mixing of two fluids from different reservoirs are responsible for the vein-type mineralization in the hydrothermal system. High K/Na, Li/Na, Cl/Br ratios, and heavy $\delta^{37}Cl$ values provide evidence for the contribution of magmatic hydrothermal fluids which may come from magmatism at depth, whereas low Cl/Br ratios and light $\delta^{37}Cl$ values imply the contribution came from surface-evaporated seawater sources. Magmatic hydrothermal fluids transporting major metals upward along faults in this region, and are mixed with evaporated seawater for ore deposition at fractures or unconformable position. In addition, we quantitively assess the fluid mixing, and the results show that the volume ratios between evaporated seawater and magmatic fluids during the Zn–Pb mineralization are between v/v = 1:9 and 4:6. This study provides new insights into the genetic models for the vein-type Zn–Pb deposits in eastern Guizhou Province, and shed light on the importance of fluid-mixing processes for triggering ore deposition.

Declaration of Competing Interest

The authors declare that they have no known competing financial interests or personal relationships that could have appeared to influence the work reported in this paper.

Acknowledgements

We are deeply grateful to Yunqi Ma, Hongwen Lin, Peng Zhang, Xiuqun Yang and Yuhong Fan for their guidance and technical support for the chemical analysis. This project was financially supported by National Natural Science Foundation of China (No. 92162214, 42103015, 42073019, 41773015, and U1812402), Key R&D Program of Yunan Province (202103AQ100003), Guizhou Provincial 2020 Science and Technology Subsidies (No. GZ2020SIG), National Key R&D Program of China (No. 2017YFC0602500), discretionary foundation of the State Key Laboratory of Nuclear Resources and Environment (Z1919), DHBK2019314, Guizhou Scientific and Technological Innovation Team (2017-5657).

Appendix A. Supplementary material

Supplementary data to this article can be found online at https://doi.org/10.1016/j.jseaes.2022.105403.

References

Andersson, S.S., Wagner, T., Jonsson, E., Fusswinkel, T., Whitehouse, M.J., 2019. Apatite as a tracer of the source, chemistry and evolution of ore-forming fluids: The case of the Olserum-Djupedal REE-phosphate mineralisation, SE Sweden. Geochim. Cosmochim. Acta 255, 163–187.

Banks, D.A., Boyce, A.J., Samson, I.M., 2002. Constraints on the origins of fluids forming Irish Zn–Pb–Ba deposits: Evidence from the composition of fluid inclusions. Econ. Geol. 97 (3), 471–480.

Banks, D.A., Gleeson, S.A., Green, R., 2000. Determination of the origin of salinity in granite-related fluids: evidence from chlorine isotopes in fluid inclusions. J. Geochem. Explor. 69, 309–312.

Beaudoin, G., Chiaradia, M., 2016. Fluid mixing in orogenic gold deposits: Evidence from the H-O–Sr isotope composition of the Val-d'Or vein field (Abitibi, Canada). Chem. Geol. 437, 7–18.

Bonifacie, M., Jendrzejewski, N., Agrinier, P., Humler, E., Coleman, M., Javoy, M., 2008. The chlorine isotope composition of Earth's mantle. Science 319 (5869), 1518–1520.

Bons, P.D., Fusswinkel, T., Gomez-Rivas, E., Markl, G., Wagner, T., Walter, B., 2014. Fluid mixing from below in unconformity-related hydrothermal ore deposits. Geology 42, 1035–1038.

Bouabdellah, M., Beaudoin, G., Leach, D.L., Grandia, F., Cardellach, E., 2009. Genesis of the Assif El Mal Zn–Pb (Cu, Ag) vein deposit. An extension-related Mesozoic vein system in the High Atlas of Morocco. Structural, mineralogical, and geochemical evidence. Miner Depos 44 (6), 689–704.

Catchpole, H., Kouzmanov, K., Putlitz, B., Seo, J.H., Fontbote, L., 2015. Zoned base metal mineralization in a porphyry system: Origin and evolution of mineralizing fluids in the Morococha district, Peru. Econ. Geol. 110 (1), 39–71.

Chen, G.Y., An, Q., Fan, Y.M., 2005. Geologic characteristic of the lead-zinc deposits in the Eastern Guizhou and analysis on metallogenesis. Guizhou Geol. 22, 252–259 in Chinese with English abstract.

Chen, S.B., Fu, J.M., Ma, L.Y., Jiang, G.X., Chen, X.Q., Lu, Y.Y., Tong, X.R., 2013. Indosinian metallogentic activity in Yuechengling-Miaoershan area, northeastern Guangxi: implications from zircon U-Pb ages and Hf isotopic constraint on ore-forming granites in Youmaling and Jiepai deposits. Geol China 40, 1189–1201 in Chinese with English abstract.

de Graaf, S., Lüders, V., Banks, D.A., Sośnicka, M., Reijmer, J.J.G., Kaden, H., Vonhof, H. B., 2020. Fluid evolution and ore deposition in the Harz Mountains revisited: isotope and crush-leach analyses of fluid inclusions. Miner. Depos. 55 (1), 47–62.

Marques de Sá, C., Noronha, F., Cardellach, E., Bobos, I., 2019. Fluid inclusion and (S, C, O, Pb) isotope study of Pb–Zn–(Cu–Ag) hydrothermal veins from Central and Northern Portugal-Metallogenic implications. Ore Geol. Rev. 112, 103043.

Eastoe, C.J., Peryt, T.M., Petrychenko, O.Y., Geisler-Cussey, D., 2007. Stable chlorine isotopes in Phanerozoic evaporites. Appl. Geochem. 22 (3), 575–588.

Eggenkamp, H.G.M., Kreulen, R., Koster Van Groos, A.F., 1995. Chlorine stable isotope fractionation in evaporites. Geochim. Cosmochim. Acta 59 (24), 5169–5175.

Eggenkamp, H.G.M., Louvat, P., Agrinier, P., Bonifacie, M., Bekker, A., Krupenik, V., Griffioen, J., Horita, J., Brocks, J.J., Bagheri, R., 2019. The bromine and chlorine isotope composition of primary halite deposits and their significance for the secular isotope composition of seawater. Geochim. Cosmochim. Acta 264, 13–29.

Fang, W.X., Hu, R.Z., Su, W.C., Xiao, J.F., Qi, L., Jiang, G.H., 2002. On intrusive ages of lamproites in Zhengyuan area, Guizhou Provience, China. Chin. Sci. Bull. 47, 307–312 in Chinese.

Fekete, S., Weis, P., Driesner, T., Bouvier, A.S., Baumgartner, L., Heinrich, C.A., 2016. Contrasting hydrological processes of meteoric water incursion during magmatic–hydrothermal ore deposition: An oxygen isotope study by ion microprobe. Earth Planet. Sci. Lett. 451, 263–271.

Fontes, J.C., Matray, J.M., 1993. Geochemistry and origin of formation brines from the Paris Basin, France: 1. Brines associated with Triassic salts. Chem. Geol. 109 (1-4), 149–175.

Fu, S., Hu, R., Batt, G.E., Danišík, M., Evans, N.J., Mi, X., 2020. Zircon (U–Th)/He thermochronometric constraints on the mineralization of the giant Xikuangshan Sb deposit in central Hunan, South China. Miner. Depos. 55 (5), 901–912.

Fusswinkel, T., Wagner, T., Wälle, M., Wenzel, T., Heinrich, C.A., Markl, G., 2013. Fluid mixing forms basement-hosted Pb–Zn deposits: Insight from metal and halogen geochemistry of individual fluid inclusions. Geology 41, 679–682.

Gao, L.Z., Chen, J.S., Dai, C.G., Ding, X.Z., Wang, X.H., Liu, Y.X., Wang, M., Zhang, H., 2014. SHRIMP zircon U-Pb dating of tuff in Fanjingshan Group and Xiajiang Group from Guizhou and Hunan Provinces and its stratigraphic implications. Geol. Bull. China 33, 949–959 in Chinese with English abstract.

Gleeson, S.A., Roberts, S., Fallick, A.E., Boyce, A.J., 2008. Micro-Fourier Transform Infrared (FT-IR) and δD value investigation of hydrothermal vein quartz: Interpretation of fluid inclusion δD values in hydrothermal systems. Geochim. Cosmochim. Acta 72, 4595–4606.

Heijlen, W., Banks, D.A., Muchez, P., Stensgard, B.M., Yardley, B.W., 2008. The nature of mineralizing fluids of the Kipushi Zn–Cu deposit, Katanga, Democratic Repubic of Congo: Quantitative fluid inclusion analysis using laser ablation ICP–MS and bulk crush-leach methods. Econ. Geol. 103, 1459–1482.

Hsu, Y.J., Zajacz, Z., Ulmer, P., Heinrich, C.A., 2019. Chlorine partitioning between granitic melt and H_2O–CO_2–NaCl fluids in the Earth's upper crust and implications for magmatic-hydrothermal ore genesis. Geochim. Cosmochim. Acta 261, 171–190.

Kusebauch, C., John, T., Barnes, J.D., Klügel, A., Austrheim, H.O., 2015. Halogen element and stable chlorine isotope fractionation caused by fluid–rock interaction (Bamble Sector, SE Norway). J. Petrol. 56, 299–324.

Large, S.J., Bakker, E.Y., Weis, P., Wälle, M., Ressel, M., Heinrich, C.A., 2016. Trace elements in fluid inclusions of sediment-hosted gold deposits indicate a magmatic-hydrothermal origin of the Carlin ore trend. Geology 44, 1015–1018.

Li, X.H., Li, W.X., Li, Z.X., Lo, C.H., Wang, J., Ye, M.F., Yang, Y.H., 2009. Amalgamation between the Yangtze and Cathaysia Blocks in South China: constraints from SHRIMP U-Pb zircon ages, geochemistry and Nd–Hf isotopes of the Shuangxiwu volcanic rocks. Precambr. Res. 174, 117–128.

Liebscher, A., Barnes, J., Sharp, Z., 2006. Chlorine isotope vapor–liquid fractionation during experimental fluid-phase separation at 400 °C/23 MPa to 450 °C/42 MPa. Chem. Geol. 234, 340–345.

Liu, A.L., Zhang, X.J., Ulrich, T., Zhang, J., Jiang, M.R., Liu, W.H., 2017. Geology, geochronology and fluid characteristics of the Pingqiu gold deposit, Southeastern Guizhou Province, China. Ore Geol. Rev. 89, 187–205.

Lüders, V., Banks, D.A., Halbach, P., 2002. Extreme Cl/Br and δ37Cl isotope fractionation in fluids of modern submarine hydrothermal systems. Miner. Depos. 37, 765–771.

Luo, C.G., Xiao, Y.K., Ma, H.Z., Ma, Y.Q., Zhang, Y.L., He, M.Y., 2012. Stable isotope fractionation of chlorine during evaporation of brine from a saline lake. Chin. Sci. Bull. 57, 1833–1843.

Mao, J.W., Li, Z.L., Ye, H.M., 2014. Mesozoic tectono-magmatic activities in South China: Retrospect and prospect. Sci. China Earth Sci. 57, 2853–2877.

Nahnybida, T., Gleeson, S.A., Rusk, B.G., Wassenaar, L.I., 2009. Cl/Br ratios and stable chlorine isotope analysis of magmatic–hydrothermal fluid inclusions from Butte, Montana and Bingham Canyon, Utah. Miner. Depos. 44, 837.

Ouyang, H.G., Mao, J.W., Santosh, M., Wu, Y., Hou, L., Wang, X.F., 2014. The Early Cretaceous Weilasituo Zn–Cu–Ag vein deposit in the southern Great Xing'an Range, northeast China: Fluid inclusions, H, O, S, Pb isotope geochemistry and genetic implications. Ore Geol. Rev. 56, 503–515.

Palero, F.J., Both, R.A., Arribas, A., Boyce, A.J., Mangas, J., Martin-Izard, A., 2003. Geology and metallogenic evolution of the polymetallic deposits of the Alcudia Valley mineral field, Eastern Sierra Morena, Spain. Econ. Geol. 98, 577–605.

Peng, J., Hu, R., Zhao, J., Fu, Y., Lin, Y., 2003. Scheelite Sm–Nd dating and quartz Ar–Ar dating for Woxi Au–Sb–W deposit, western Hunan. Chin. Sci. Bull. 48, 2640–2646.

Qin, Y.J., Du, Y.S., Mou, J., Lu, D.B., Long, J.X., Wang, A.H., Zhang, H.S., Zeng, C.X., 2015. Geochronology of Neoproterozoic Xiajiang Group in southeast Guizhou, South China, and Its geological implication. Earth Sci.-J. China Univ. Geosci. 40, 1107–1120 in Chinese with English abstract.

Richard, A., Banks, D.A., Mercadier, J., Boiron, M.C., Cuney, M., Cathelineau, M., 2011. An evaporated seawater origin for the ore-forming brines in unconformity-related uranium deposits (Athabasca Basin, Canada): Cl/Br and δ37Cl analysis of fluid inclusions. Geochim. Cosmochim. Acta 75, 2792–2810.

Rusk, B.G., Reed, M.H., Dilles, J.H., 2008. Fluid inclusion evidence for magmatic-hydrothermal fluid evolution in the porphyry copper-molybdenum deposit at Butte, Montana. Econ. Geol. 103, 307–334.

Samson, I.M., Williams-Jones, A.E., Ault, K.M., Gagnon, J.E., Fryer, B.J., 2008. Source of fluids forming distal Zn–Pb–Ag skarns: Evidence from laser ablation–inductively coupled plasma–mass spectrometry analysis of fluid inclusions from El Mochito, Honduras. Geology 36, 947–950.

Seo, J.H., Zajacz, Z., 2016. Fractionation of Cl/Br during fluid phase separation in magmatic–hydrothermal fluids. Geochim. Cosmochim. Acta 183, 125–137.

Shu, Q., Chang, Z., Hammerli, J., Lai, Y., Huizenga, J.M., 2017. Composition and evolution of fluids forming the baiyinnuo'er Zn–Pb skarn deposit, northeastern china: insights from laser ablation icp–ms study of fluid inclusions. Econ. Geol. 112, 1441–1460.

Song, H., Xu, Z.Q., Ni, S.J., Zhang, C.J., Liang, J., Chen, F.G., Tang, C.Y., 2015. Response of the Motianling Granitic Pluton in North Guangxi to the Tectonic Evolution in the Southwestern Section of the Jiangnan Orogenic Belt: Constraints from Neoproterozoic Zircon Geochronology. Geotectonica et Metallogenia 39, 1156–1171 in Chinese with English abstract.

Van Daele, J., Hulsbosch, N., Dewaele, S., Boiron, M.C., Piessens, K., Boyce, A., Muchez, P., 2018. Mixing of magmatic-hydrothermal and metamorphic fluids and the origin of peribatholitic Sn vein-type deposits in Rwanda. Ore Geol. Rev. 101, 481–501.

Walter, B.F., Kortenbruck, P., Scharrer, M., Zeitvogel, C., Wälle, M., Mertz-Kraus, R., Markl, G., 2019. Chemical evolution of ore-forming brines–Basement leaching, metal provenance, and the redox link between barren and ore-bearing hydrothermal veins. A case study from the Schwarzwald mining district in SW-Germany. Chem. Geol. 506, 126–148.

Wang, L., Zhang, Y.W., Liu, S.G., 2009. The application of regional gravity and magnetic data to delineating intrusivie bodies and local geological structures in Guizhou Province. Geophys Geochem Explor 33, 245–250 in Chinese with English abstract.

Wang, X.L., Zhou, J.C., Griffin, W.A., Wang, R.C., Qiu, J.S., O'reilly, S.Y., Zhang, G.L., 2007. Detrital zircon geochronology of Precambrian basement sequences in the Jiangnan orogen: dating the assembly of the Yangtze and Cathaysia Blocks. Precambr. Res. 159, 117–131.

Wang, Y.J., Fan, W.M., Zhang, G.W., Zhang, Y.H., 2013. Phanerozoic tectonics of the South China Block: key observations and controversies. Gondwana Res. 23, 1273–1305.

Wilkinson, J.J., 2001. Fluid inclusions in hydrothermal ore deposits. Lithos 55, 229–272.

Williams-Jones, A.E., Samson, I.M., Ault, K.M., Gagnon, J.E., Fryer, B.J., 2010. The genesis of distal zinc skarns: Evidence from the Mochito deposit, Honduras. Econ. Geol. 105, 1411–1440.

Xiao, Y.K., Zhang, C.G., 1992. High precision isotopic measurement of chlorine by thermal ionization mass spectrometry of the Cs_2Cl^+ ion. Int. J. Mass Spectrom. 116, 183–192.

Xiong, Y.Q., Shao, Y.J., Mao, J.W., Wu, S.C., Zheng, M.H., 2019. The polymetallic magmatic-hydrothermal Xiangdong and Dalong systems in the W-Sn–Cu–Pb–Zn–Ag Dengfuxian orefield, SE China: constraints from geology, fluid inclusions, H–O–S–Pb isotopes, and sphalerite Rb–Sr geochronology. Miner. Depos. 54, 1101–1124.

Xu, D.R., Deng, T., Chi, G.X., Wang, Z., Zou, F., Zhang, J., Zou, S.H., 2017. Gold mineralization in the Jiangnan Orogenic Belt of South China: Geological, geochemical and geochronological characteristics, ore deposit-type and geodynamic setting. Ore Geol. Rev. 88, 565–618.

Xu, L., Luo, C.G., Wen, H.J., Zhou, Z.B., Qin, C.J., 2018. Origin of ore-forming fluids of the Zn–Pb–(Cu) deposits in the Jinbao mine district of eastern Guizhou Province, China: Evidence from chemical compositions of fluid inclusions and their lithium isotopes. Geochem. J. 52, 483–496.

Xu, L., Luo, C.G., Wen, H.J., Deng, M.G., Qin, C.J., Zhu, C.W., Fourestier, J., 2021. Lithium and chlorine isotopic constraints on fluid sources and evolution at the Luziyuan distal skarn Zn–Pb–Fe–(Cu) deposit, western Yunnan Province. China. Ore Geol Rev 133, 104057.

Yang, D., Hou, Z.Q., Zhao, Y., Hou, K.J., Yang, Z.M., Tian, S.H., Fu, Q., 2015. Lithium isotope traces magmatic fluid in a seafloor hydrothermal system. Sci. Rep. 5, 13812.

Yang, Z.W., Liu, L., 2014. The isotopic geochemical feature and genies of Pb–Zn deposit in Zhengyuan area, Guizhou. Yunnan Geol. 33, 503–507 in Chinese with English abstract.

Yao, J.L., Shu, L.S., Santosh, M., Li, J.Y., 2012. Precambrian crustal evolution of the South China Block and its relation to supercontinent history: constraints from U-Pb ages, Lu–Hf isotopes and REE geochemistry of zircons from sandstones and granodiorite. Precambr. Res. 208, 19–48.

Yardley, B.W.D., Bodnar, R.J., 2014. Fluids in the continental crust. Geochem. Perspect. 2014 (3), 1–2.

Ye, L., Cook, N.J., Liu, T., Ciobanu, C.L., Gao, W., Yang, Y., 2012. The Niujiaotang Cd-rich zinc deposit, Duyun, Guizhou province, southwest China: ore genesis and mechanisms of cadmium concentration. Miner Depos 47, 683–700.

Zhai, D.G., Liu, J.J., Zhang, H.Y., Tombros, S., Zhang, A.L., 2018. A magmatic-hydrothermal origin for Ag–Pb–Zn vein formation at the Bianjiadayuan deposit, inner Mongolia, NE China: Evidences from fluid inclusion, stable (C–H–O) and noble gas isotope studies. Ore Geol. Rev. 101, 1–16.

Zhao, J.H., Zhou, M.F., Yan, D.P., Zheng, J.P., Li, J.W., 2011. Reappraisal of the ages of Neoproterozoic strata in South China: no connection with the Grenvillian orogeny. Geology 39, 299–302.

Zhou, Z.B., Wen, H.J., Qin, C.J., Liu, L., 2017. Geochemical and isotopic evidence for a magmatic-hydrothermal origin of the polymetallic vein-type Zn–Pb deposits in the northwest margin of Jiangnan Orogen, South China. Ore Geol. Rev. 86, 673–691.

Zhou, Z.B., Wen, H.J., 2021. A magmatic-hydrothermal indium-bearing polymetallic vein mineralization belt in the western Jiangnan Orogen: Evidence from zinc and cadmium isotopes of sphalerite. Ore Geol. Rev. 131, 103843.